Received: 1 July 2023 | Accepted: 22 August 2023

DOI: 10.1002/pamm.202300209

RESEARCH ARTICLE

Numerical simulation of miscible multiphase flow and fluid–fluid interaction in deformable porous media

Sven Peters | **Yousef Heider** | **Bernd Markert**

Institute of General Mechanics, RWTH Aachen University, Aachen, Germany

Correspondence
Yousef Heider, Institute of General Mechanics, RWTH Aachen University. Eilfschornsteinstr. 18, 52062 Aachen, Germany.
Email: heider@iam.rwth-aachen.de

Funding information
German Research Foundation, Grant/Award Number: 458375627

Abstract

The focus of the underlying research work is on the macroscopic modeling of unstable multiphase fluid flow in deformable porous media, where a lower-viscous fluid is displaced by a more viscous fluid. This process leads to the formation of channel-like networks, called viscous fingering. The instability effect is involved in a wide range of different fields in engineering. Some of the most common applications include carbon sequestration to store carbon dioxide (CO_2) in underground reservoirs, contaminant transport in geostructures, in industrial processes, such as filtration, catalytic reactions, and in the operation of polymer electrolyte membrane fuel cells with multiphase flow in the gas diffusion layers. In this work, ideal miscible water–glycerin fluids are considered. It is assumed that the interacting fluids in the deformable porous media are incompressible. In addition, a dispersion–diffusion law is applied to capture the fluid–fluid interactions. The presence of a deformable porous material adds additional effects to the problem of the multiphase flow in porous media. The stresses in the porous solid matrix lead to changes in the porosity and influence the flow velocity of the fluids. To couple the deformable porous media with the multiphase flow, a macroscopic approach is used that relies on the theory of porous media. For the porous solid matrix, a linear elastic material model within small strains assumption is applied. The influence of the deformation-dependent porosity on the instability is studied for 2D simulations, such as a multilayered geometry with different elastic parameters. The presented coupled nonlinear system of differential equations is simulated with the finite element method. Furthermore, a stabilization technique based on the quasi-compressibility method is used.

KEYWORDS
fluid–fluid interaction, multiphase fluid flow, poromechanics, TPM, viscous fingering

1 | INTRODUCTION

Many engineering applications and processes are related to the fluid–fluid interaction in deformable porous media. These include contaminant transport, carbon dioxide (CO_2) storage in groundwater reservoirs [1], industrial processes like filtration and catalytic reactions, and unsaturated soil hydro-mechanical response with interacting water–air phases, see, for example, [2, 3] for references. For the mentioned multi-phase flow applications in porous media, instabilities at the fluid–fluid interface can happen. One instability effect is called *"viscous fingering"* and occurs when a *lower*-viscous fluid displaces a *higher*-viscous fluid. This effect forms channel-like networks and it is independent of the fluid's miscibility.

One of the earliest works about the fluid fingering effect goes back to Saffman and Taylor [4] and Chuoke et al. [5]. They investigated experiments for immiscible fluids in porous media or Hele–Shaw cells, which were compared with linear stability analysis. A historical review for miscible and immiscible viscous fingering is written in Homsy [6]. In general, the effect of viscous fingering has been widely studied experimentally in the literature, as can be found for instance in the works of [6–9]. In Suekane et al. [8], they studied the three-dimensional viscous fingering in a packed bed of polymeric particles for different Peclet numbers and viscosity contrasts. They successfully compared their experimental results with a linear stability analysis present in Tan and Homsy [15] based on a quasi-steady-state approximation (QSSA) in a rectangular domain.

From the mathematical modeling aspect, pore-scale approaches [10, 13–16] and macroscopic approaches [11] can widely be found in the literature. In Zimmerman and Homsy [14], the nonlinear behavior of dispersion-dependent viscous fingering is studied, where the *splitting* and *coalescence* of fingers can be observed using different nonlinear simulations. Their simulation results showed that the splitting of the fingertips only occurs when a stability limit is reached, which is consistent with the results from Tan and Homsy [15] for a scalar-valued and constant diffusion–dispersion parameter.

The current research work focuses on the macroscopic modeling of a miscible fluid–fluid interaction based on the fundamentals of multiphase continuum mechanics. For this, a *water–glycerine* mixture is considered, which is idealized as incompressible phases and can mix by molecular diffusion and dispersion in the porous medium. For a detailed description of dispersion and molecular diffusion in porous media, the reader is referred to Bear [12]. During the mathematical modeling, a second-order diffusion–dispersion tensor is utilized to describe this process [12]. The fluid mixture viscosity depends on the concentration of the solution and an exponential approach is applied, which has been used in many nonlinear simulations [13–16].

The models in the previously listed literature focus merely on the fluid flow and neglect the deformation of the porous medium. However, the consideration of porous media deformation allows for exploring new applications. This includes, for instance, the simulation of hydraulic fracturing of multiphase porous media using the phase-field approach in addition to utilizing machine learning schemes to generate constitutive models that capture the deformation-dependent response, see, for example, [2, 17, 18] for more details. To couple the fluid mixture with the deformable solid, a macroscopic continuum mechanical approach is used based on the *theory of porous media* (TPM) [19–21]. For the solid continuum, we assume a geometrical and material linearity response by using Hook's law. The momentum of the fluid mixture is described by Darcy's law with a deformation-dependent permeability. In this case, we use an isotopic deformation-dependent permeability tensor. For more details, the interested reader is referred to Markert [22].

To give an overview, the paper is organized according to the following structure. In Section 2, the multiphase porous media model is developed based on the TPM with the relevant homogenization fundamentals, constitutive equations, and model assumptions. Thereafter, Section 3 presents a summary of the governing equations and the applied numerical method. Thereafter, a numerical example is solved in Section 4, which considers a layered porous domain with layers that have different elasticity moduli and permeability parameters. To realize the viscous fingering and the deformation-dependent permeability effect, water is injected into a water–glycerine solution and the deformation of the solid is studied. In the end, concluding remarks are presented in Section 5.

2 | THEORETICAL FUNDAMENTALS

Based on the TPM [19, 20], homogenization is applied to the heterogeneous multiphase porous material, leading to a continuum and homogeneous medium φ with superimposed and interacting phases. These phases include the solid phase (φ^S) and two-fluid phases, which are water (φ^W) and glycerine (φ^G). Thus, $\varphi = \varphi^S \cup \varphi^F$ with $\varphi^F = \varphi^W \cup \varphi^G$. Following

this, the local volume fractions are defined as $n^\alpha = dv^\alpha/dv$ with dv^α being the partial volume element and dv is the bulk volume element. Thus, the saturation condition can be defined as $1 = n^S + n^F$ with n^S being the solidity and n^F being the porosity.

The definition of the volume fractions leads to two different density formulations with $\rho^{\alpha R} = \mathrm{d}m^\alpha/\mathrm{d}v^\alpha$ as the intrinsic or material density and $\rho^\alpha = \mathrm{d}m^\alpha/\mathrm{d}v = n^\alpha \rho^{\alpha R}$ is the partial density. For the fluid mixture, a material density ρ^{FR} and a partial density $\rho^F = n^F \rho^{FR}$ are also defined. The fluid material density ρ^{FR} is an average value of the water–glycerine material densities and depends on the composition of the fluid mixture. To characterize the local composition of the fluid mixture, a local mass concentration c^β with $\beta \in \{W, G\}$ is used and expressed as

$$c^\beta = \frac{\mathrm{d}m^\beta}{\mathrm{d}m^F} = \frac{\rho^\beta}{\rho^F}\,, \qquad 1 = c^W + c^G\,, \qquad \frac{1}{\rho^{FR}} = \frac{c^W}{\rho^{WR}} + \frac{c^G}{\rho^{GR}}\,. \tag{1}$$

Following this, the constituent local mass and momentum balance equations are specified as

$$\hat{\rho}^\alpha = (\rho^\alpha)'_\alpha + \rho^\alpha \operatorname{div} \mathbf{v}_\alpha\,, \qquad \rho^\alpha (\mathbf{v}_\alpha)'_\alpha = \operatorname{div}(\mathbf{T}^\alpha) + \hat{\mathbf{p}}^\alpha\,. \tag{2}$$

Herein, $\mathbf{v}_\alpha$ is the constituent velocity, $\mathbf{T}^\alpha$ is the Cauchy stress tensor, $\hat{\mathbf{p}}^\alpha$ is the momentum exchange vector, and $\hat{\rho}^\alpha$ is the mass production term. The material time derivative with respect to the motion of a constituent φ^α is expressed as $(\bullet)'_\alpha$. In this work, the modeling framework proceeds from the following assumptions:

1. No mass exchange between the solid and the fluid phases: $\hat{\rho}^\alpha = 0$.
2. The solid and the fluid phases are materially incompressible, that is, constant material densities with $\rho^{\alpha R} = \text{const.}$
3. Equal and constant material densities of the water and glycerine phases, that is, $\rho^{WR} \approx \rho^{GR}$, which means that the density of the fluid mixture ρ^{FR} is also constant according to Equation (1).
4. Geometrically linear framework with the linear solid strain tensor $\boldsymbol{\varepsilon}_S$ for the kinematics.
5. Quasi-static conditions with $\rho^\alpha (\mathbf{v}_\alpha)'_\alpha \approx \mathbf{0}$.
6. Isothermal processes with negligible temperature changes.

Based on the aforementioned model assumptions, the density can be eliminated from the balance equations in Equation (2). Thus, the governing balance equations for the solid, fluid mixture and the overall aggregate can be summarized as follows:

$$\begin{array}{lll} & \text{Volume balance} & \text{Linear momentum balance} \\ \text{Overall aggregate}: & 0 = \operatorname{div} \mathbf{w}_F + \operatorname{div} \mathbf{v}_S & \mathbf{0} = \operatorname{div}(\boldsymbol{\sigma}^S + \mathbf{T}^F) \\ \text{Fluid mixture}: & 0 = (n^F)'_F + n^F \operatorname{div} \mathbf{v}_F & \mathbf{0} = \operatorname{div} \mathbf{T}^F + \hat{\mathbf{p}}^F \\ \text{Solid component}: & 0 = (n^S)'_S + n^S \operatorname{div} \mathbf{v}_S & \mathbf{0} = \operatorname{div} \boldsymbol{\sigma}^S + \hat{\mathbf{p}}^S \end{array} \tag{3}$$

In this, $\mathbf{w}_F = n^F(\mathbf{v}_F - \mathbf{v}_S)$ is the filter velocity, and the momentum production terms fulfill the constraint $\hat{\mathbf{p}}^S + \hat{\mathbf{p}}^F = \mathbf{0}$ during the deformation process. Additionally, $\boldsymbol{\sigma}^S$ is the total solid stress tensor and $\mathbf{T}^F$ is the total fluid stress tensor.

For constitutive modeling, the concept of effective stresses is applied, which provides a framework for analyzing the stress state at a material point. In particular, the total stress consists of an "extra" or "effective" stress and a weighted pore-fluid pressure term p. For effective stresses, thermodynamically consistent formulations need to be formulated. Based on this, the stress quantities can be expressed as

$$\boldsymbol{\sigma}^S = \boldsymbol{\sigma}^S_E - n^S p\, \mathbf{I}\,, \qquad \mathbf{T}^F = \mathbf{T}^F_E - n^F p\, \mathbf{I}\,, \qquad \hat{\mathbf{p}}^F = \hat{\mathbf{p}}^F_E - p \operatorname{grad} n^F\,. \tag{4}$$

The solid effective stress $\boldsymbol{\sigma}^S_E$ for a linear elastic material model can be expressed as

$$\boldsymbol{\sigma}^S_E = \kappa^S (\operatorname{tr} \boldsymbol{\varepsilon}_S)\, \mathbf{I} + 2\mu^S \boldsymbol{\varepsilon}^D_S \quad \text{with} \quad \boldsymbol{\varepsilon}_S := \frac{1}{2}(\operatorname{grad} \mathbf{u}_S + \operatorname{grad}^T \mathbf{u}_S)\,. \tag{5}$$

Herein, $\mathbf{u}_S$ is the solid displacement, $\kappa^S := \lambda^S + 2/3\mu^S$ is the bulk modulus, and λ^S, μ^S are the first and second Lamé constants. Additionally, $\boldsymbol{\varepsilon}^D_S$ is the deviatoric part of the linear strain tensor $\boldsymbol{\varepsilon}_S$. With the assumption that the fluid–wall

TABLE 1 Summary of the governing equations in the strong form.

Overall mass balance:	$0 = \operatorname{div} \mathbf{w}_F + \operatorname{div} \mathbf{v}_S - \epsilon \, \Delta \, p$
Overall momentum balance:	$\mathbf{0} = \operatorname{div}(\boldsymbol{\sigma}_E^S - p\mathbf{I})$
Fluid mixture momentum balance:	$\mathbf{0} = \mathbf{w}_F + (\eta^{FR})^{-1}\mathbf{K}^S \operatorname{grad} p$
Water transport equation:	$0 = n^F (c^W)'_S + \operatorname{grad} c^W \cdot \mathbf{w}_F - \operatorname{div}(n^F \mathbf{D} \operatorname{grad} c^W)$

friction on the pore scale is dominating the interaction between the solid and the fluid constituents, that is, $|\operatorname{div} \mathbf{T}_E^F| \ll |\hat{\mathbf{p}}_E^F|$, the contribution of the fluid effective stress tensor can be neglected from the fluid momentum balance $\operatorname{div} \mathbf{T}_E^F \approx \mathbf{0}$, see, for example, [22]. For the interaction force $\hat{\mathbf{p}}_E^F$, the following linear constitutive equation is selected, whereas the fluid momentum balance (3) results in Darcy's law. In particular, $\hat{\mathbf{p}}_E^F$ is expressed as

$$\hat{\mathbf{p}}_E^F = -n^F \eta^{FR} (\mathbf{K}^S)^{-1} \mathbf{w}_F \tag{6}$$

$$\text{with} \quad \eta^{FR} = \tilde{\eta}(c^W) = \eta^{WR} \mathrm{e}^{R(1-c^W)} \quad \text{and} \quad R = \ln\left(\frac{\eta^{GR}}{\eta^{WR}}\right). \tag{7}$$

Thereby, η^{FR} is the fluid mixture viscosity that depends on the concentration c^W. Following [13, 15, 16], an exponential law is chosen to describe the concentration-dependent fluid viscosity. The parameters η^{WR} and η^{GR} are the water and glycerine viscosities, respectively. The intrinsic permeability tensor $\mathbf{K}^S$ is considered in this work as isotropic and deformation dependent. The deformation dependency is realized by formulating the permeability as a function of the porosity. Thus, having K_0^S as the intrinsic permeability parameter, the intrinsic permeability tensor according to [22] can be expressed as

$$\mathbf{K}^S = K^S(n^F)\,\mathbf{I} = K_0^S \left(\frac{n^F}{n_{0S}^F} \frac{1 - n_{0S}^F}{1 - n^F} \right)^{\kappa} \mathbf{I} \tag{8}$$

with κ as a model fitting parameter and n_{0S}^F as the initial porosity. For the calculation of the porosity, a linearized solution of the solidity can be used, that is, $n^S \approx n_{0S}^S (1 - \operatorname{div} \mathbf{u}_S)$, which results from the solid volume balance (3), see, for example, [23].

The solute transportation is described with the water transport equation

$$n^F (c^W)'_F = \operatorname{div}(n^F \mathbf{d}_{WF}) \quad \text{with} \quad n^F \mathbf{d}_{WF} = n^F (\mathbf{v}_W - \mathbf{v}_F). \tag{9}$$

In this, $n^F \mathbf{d}_{WF}$ represents the diffusion mass flux. For this mass flux, a constitutive equation is adopted to describe the diffusion–dispersion relationship between the water–glycerin solution in the porous medium [12]:

$$n^F \mathbf{d}_{WF} = n^F \mathbf{D} \operatorname{grad} c^W \quad \text{with} \quad \mathbf{D} = D_m \mathbf{I} + a_T |\mathbf{w}_F| \, \mathbf{I} + (a_L - a_T) \frac{\mathbf{w}_F \otimes \mathbf{w}_F}{|\mathbf{w}_F|}, \tag{10}$$

where $\mathbf{D}$ is the diffusion–dispersion tensor. The coefficients D_m, a_L, and a_T are related to molecular diffusion. The second and third coefficients are called longitudinal and transversal dispersivity coefficients and they depend in general on the properties of the porous medium and on the fluid mixture velocity. For simplicity in this work, constant dispersivity coefficients are considered which are independent of the fluid velocity.

3 | GOVERNING EQUATIONS AND NUMERICAL IMPLEMENTATION

This section describes the numerical method for solving the initial boundary value problem (IBVP) using the Bubnov–Galerkin approach with the finite element method (FEM). Starting with the primary variables $\boldsymbol{\xi} = \{\mathbf{u}_S, \mathbf{w}_F, p, c^W\}$, the governing equations in the strong form needed to solve boundary-value problems are summarized in Table 1. These include

TABLE 2 Material parameters for the fluids and solid phases.

Solid				Fluid		
Parameter	**Unit**	**Value Layer 1**	**Value Layer 2**	**Parameter**	**Unit**	**Value**
n_{0S}^S	–	0.6	0.6	R	–	7.3
ν^S	–	0.3	0.3	η^{WR}	Pa s	$1 \cdot 10^{-3}$
E^S	MPa	$2 \cdot 10^3$	$10\,E^{S1}$	D_m	cm^2/s	$1 \cdot 10^{-7}$
K_0^S	cm^2	$3 \cdot 10^{-11}$	$1/3\,K_0^{S1}$	a_L	cm	$0.99 \cdot 10^{-2}$
κ	–	1.0	1.0	a_T	cm	$0.49 \cdot 10^{-2}$

the *overall mass balance*, the *overall momentum balance*, the *fluid mixture momentum balance*, and the *water transport balance equation*.

The IBVP is solved by using the software package FlexPDE (version 7.20). For spatial discretization, triangular elements are used with quadratic shape functions. A second-order implicit backward difference formula is used for the discretization in time. To reduce the calculation time, a staggered and monolithic time-stepping scheme is used. First, for each iteration step, the coupled solution of the pressure, solid displacement, and filter velocity are calculated. After solving the coupled system, the water transport equation is solved in a later step. To satisfy the *inf–sup* condition for the case of low permeability and/or incompressible pore fluid, a quasi-compressibility method is used for the overall mass balance. Here in Table 1 in blue a pressure-Laplacian term is added with $\epsilon \ll 1$ as a regularization parameter [24, 25].

4 | NUMERICAL SIMULATION

In this part, a simulation is realized on a layered porous structure with different material parameters that are summarized in Table 2. The parameters of the fluids are counted based on experiments presented in [7, 8].

The geometry (length $b = 10\,cm$ and height $a = 7.5\,cm$) together with the boundary conditions is illustrated in Figure 1(a). In particular, the structure has three porous layers with two different material properties, where layer (2) is stiffer and less permeable than the middle layer (1). At the inlet, water is injected with $c^W = 1.0$ and the velocity of $w_F = 10^{-3}\,cm/s$. At the outlet, a drained boundary with the pressure $p = 0$ is adopted. For the initial condition, a water–glycerin solution is assumed with a concentration $c_0^W = \tilde{c}(t = t_0, \mathbf{x}) = 0.7$. The viscosity contrast between the injected water and the defending water–glycerin solute results in $M = 8.9$, which can be calculated by Equation (7). The initial values of the velocity are defined as $\mathbf{w}_{F0} = \mathbf{0}$ and for the pressure $p_0 = 0$. To avoid a strong concentration gradient and a dominant convective term in the water transport equation, the velocity and the concentration on the inlet are increased linearly in the interval of $t \in [0, 100]\,s$ from the initial condition to the assigned boundary condition.

In Figure 1(b), the concentration field of the IBVP is shown for the times 500, 1500, and 2500 s. At the time of 500 s, the flow of water is localized between the layers. The water flows from the more impermeable layer into the permeable layer that leads to the preferred flow, whereas the instability leads to increasing the observed localized flow of the water. Thereby, the *shielding* is observed in the middle of the first layer and the fingers will start to grow [14]. For later times at 1500 and 2500 s, multiple *coalescence* and *finger-tip splitting* are noted. In total, the multiple splitting and merging of the fingers occur because a certain stability limit is exceeded in the system with too large Peclet numbers and viscosity contrasts [15].

In the next step, the deformation of the porous material due to the two-phase fluid flow is studied. For this, the permeability change along the path $\overline{AB}$, illustrated in Figure 1(a), is investigated. The interaction between the solid and the fluid phases leads to the deformation of the porous matrix according to the interaction force (7), which is also a time-dependent process. The deformation-dependent permeability at different times is shown in Figure 1(c).

For the simulation results, the permeability change along the path is highest at the beginning of the simulation, because there is more of the water–glycerin solution in the porous body, which leads to a higher pressure gradient. Thereafter, at 1500 s, the pressure gradient decreases and the change of the porosity on the part becomes smaller. The influence of the fingers on the deformation is small for the chosen parameters because the viscosity contrast is not significant. An increase in the viscosity contrast leads to an enormous increase in the computational cost, as the *finger-tip splitting* and *coalescence* require a fine mesh resolution.

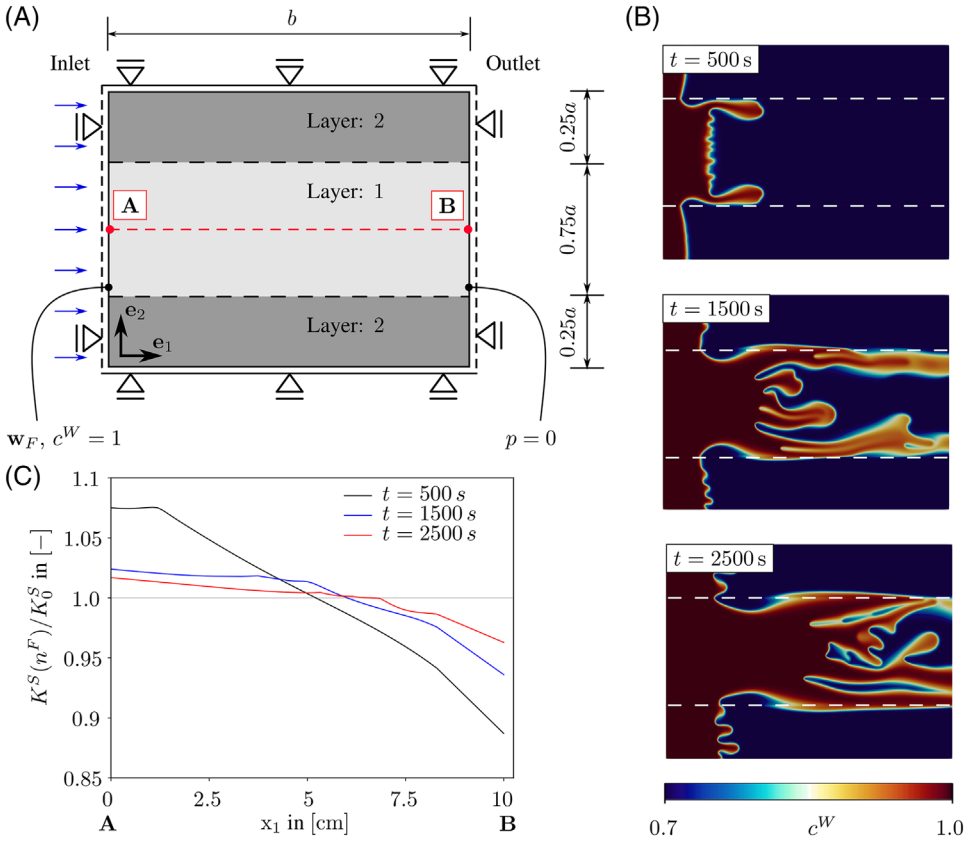

FIGURE 1 (A) The geometry and boundary conditions of the initial-boundary-value problem. (B) Simulation results of the water concentration at different times of the computation. (C) Plots of the deformation-dependent permeability along the path $\overline{AB}$ at different times.

5 | CONCLUSIONS

In this work, a model is developed for miscible multi-phase transport in deformable porous media based on the TPM. For the fluid–fluid interaction, which considered water and glycerin as an example, a diffusion–dispersion tensor is used, whereas the fluid–solid interaction is realized in the balance equations through the effective stresses. The extension of the rigid viscous fingering models to deformable porous media opens many new applications, such as the coupling of inelastic deformations or fracturing.

In the numerical implementation using the FEM, the underlying study applied a stable numerical solution with the quasi-compressibility method to satisfy the *inf–sup* condition.

The viscous fingering is investigated in layered porous media with different material properties. For the selected viscosity contrast between the two fluids, the viscous fingering affected slightly the deformation of the porous medium, where the pressure gradient is the driving force for this deformation. Future works on this topic will address the effect of fluid–fluid flow with high viscosity contrast on both the numerical stability and the deformation of the porous domain. The effect of externally induced solid deformation on the viscous fingering formation will also be addressed in future works.

ACKNOWLEDGMENTS

The authors would like to gratefully thank the German Research Foundation (DFG) for the support of the project "Multi-field continuum modeling of two-fluid-filled porous media fracture augmented by microscale-based machine-learning material laws", grant number 458375627.

Open access funding enabled and organized by Projekt DEAL.

ORCID

Yousef Heider https://orcid.org/0000-0003-2281-2563

REFERENCES

1. Szulczewski, M. L., MacMinn, C. W., Herzog, H. J., & Juanes, R. (2012). Lifetime of carbon capture and storage as a climate-change mitigation technology. *Proceedings of the National Academy of Sciences*, *109*, 5185–5189.
2. Heider, Y., & Sun, W. (2020). A phase field framework for capillary-induced fracture in unsaturated porous media: Drying-induced vs. hydraulic cracking. *Computer Methods in Applied Mechanics and Engineering*, *359*, 112647.
3. Heider, Y., Suh, H. S., & Sun, W. C. (2021). An offline multi-scale unsaturated poromechanics model enabled by self-designed/self-improved neural networks. *International Journal for Numerical and Analytical Methods in Geomechanics*, *45*, 1212–1237.
4. Saffman, P. G., & Taylor, G. I. (1958). The penetration of a fluid into a porous medium or Hele–Shaw cell containing a more viscous liquid. *Proceedings of the Royal Society of London. Series A. Mathematical and Physical Sciences*, *245*, 312–329.
5. Chuoke, R. L., Van Meurs, P., & van der Poel, C. (1959). The instability of slow, immiscible, viscous liquid–liquid displacements in permeable media. *Transactions of the AIME*, *216*, 188–194.
6. Homsy, G. M. (1987). Viscous fingering in porous media. *Annual Review of Fluid Mechanics*, *19*, 271–311.
7. Malhotra, S., Sharma, M. M., & Lehman, E. R. (2015). Experimental study of the growth of mixing zone in miscible viscous fingering. *Physics of Fluids*, *27*, 014105.
8. Suekane, T., Ono, J., Hyodo, A., & Nagatsu, Y. (2017). Three-dimensional viscous fingering of miscible fluids in porous media. *Physical Review Fluids*, *2*, 103902.
9. Tan, C., & Homsy, G. M. (1986). Stability of miscible displacements in porous media: Rectilinear flow. *The Physics of Fluids*, *29*, 3549–3556.
10. Chaaban, M., Heider, Y., & Markert, B. (2022). A multiscale lbm–tpm–pfm approach for modeling of multiphase fluid flow in fractured porous media. *International Journal for Numerical and Analytical Methods in Geomechanics*, *46*, 2698–2724.
11. Gomez, H., Cueto-Felgueroso, L., & Juanes, R. (2013). Three-dimensional simulation of unstable gravity-driven infiltration of water into a porous medium. *Journal of Computational Physics*, *238*, 217–239.
12. Bear, J. (1988). *Dynamics of fluids in porous media*. Dover.
13. Zimmerman, W. B., & Homsy, G. M. (1992). Viscous fingering in miscible displacements: Unification of effects of viscosity contrast, anisotropic dispersion, and velocity dependence of dispersion on nonlinear finger propagation. *Physics of Fluids A: Fluid Dynamics*, *4*, 2348–2359.
14. Zimmerman, W. B., & Homsy, G. M. (1991). Nonlinear viscous fingering in miscible displacement with anisotropic dispersion. *Physics of Fluids A: Fluid Dynamics*, *3*, 1859–1872.
15. Tan, C., & Homsy, G. M. (1988). Simulation of nonlinear viscous fingering in miscible displacement. *The Physics of Fluids*, *31*, 1330–1338.
16. Nijjer, J. S., Hewitt, D. R., & Neufeld, J. A. (2018). *The dynamics of miscible viscous fingering from onset to shutdown* (vol. 837, pp. 520–545). Cambridge University Press.
17. Heider, Y. (2021). A review on phase-field modeling of hydraulic fracturing. *Engineering Fracture Mechanics, Engineering Fracture Mechanics*, *253*, 107881.
18. Heider, Y. (2021). Multi-field and multi-scale computational fracture mechanics and machine-learning material modeling, Habilitation. Report No. IAM-13, RWTH Aachen University. DOI: https://doi.org/10.18154/RWTH-2021-10362
19. de Boer, R. (2000). *Theory of porous media*. Springer-Verlag, Berlin.
20. Ehlers, W. (2002). *Foundations of multiphasic and porous materials*. Springer.
21. Ehlers, W., & Wagner, A. (2019). Modelling and simulation methods applied to coupled problems in porous-media mechanics. *Archive of Applied Mechanics*, *89*, 609–628.
22. Markert, B. (2007). A constitutive approach to 3D nonlinear fluid flow through finite deformable porous continua. *Transport in Porous Media*, *70*, 427–450.
23. Heider, Y., & Markert, B. (2017). A phase-field modeling approach of hydraulic fracture in saturated porous media. *Mechanics Research Communications*, *80*, 38–46.
24. Guermond, J. L., & Quartapelle, L. (2010). On stability and convergence of projection methods based on pressure Poisson equation. *International Journal for Numerical Methods in Fluids*, *26*, 1341–1383.
25. Markert, B., Heider, Y., & Ehlers, W. (2010). Comparison of monolithic and splitting solution schemes for dynamic porous media problems. *International Journal for Numerical Methods in Engineering*, *82*, 1341–1383.

How to cite this article: Peters, S., Heider, Y., & Markert, B. (2023). Numerical simulation of miscible multiphase flow and fluid–fluid interaction in deformable porous media. *Proceedings in Applied Mathematics and Mechanics*, *23,* e202300209. https://doi.org/10.1002/pamm.202300209